Interference and Outage Analysis of Random D2D Networks Underlaying Millimeter-Wave Cellular Networks

Sachitha Kusaladharma, Zhang Zhang, and Chintha Tellambura, *Fellow, IEEE*

***Abstract*— Device-to-device (D2D) networks underlaying a millimeter-wave cellular network have great potential for capacity growth. Thus, it is important to characterize the outage of such a D2D link incorporating millimeter-wave propagation effects, user association rules, power control, and spatial randomness. To this end, we model the locations of cellular transmitters and receivers as homogeneous Poisson point processes and those of the D2D nodes as a Matérn cluster process, and incorporate blockages due to random objects, sectored antenna patterns, log-distance path loss, and Nakagami-m fading. Furthermore, we consider antenna gain inversion-based power control, and peak power constraints for D2D devices along with distinct path loss exponents and distinct fading severities for line-of-sight (LOS) and non-LOS scenarios. With the aid of stochastic geometry tools, we derive closed-form expressions of the moment generating function of the aggregate interference on a D2D receiver node and its outage probability for two transmitter–receiver association schemes—nearest association and LOS association. We finally show that the feasibility of millimeter-wave D2D communication relies heavily on the D2D cluster radii, peak power thresholds, and node densities. Furthermore, these parameters affect the performance of the desired link more than the interference and noise.**

***Index Terms*— Millimeter wave networks, D2D networks, stochastic geometry, aggregate interference.**

I. Introduction

THE FIFTH GENERATION (5G) of cellular standards promises high capacity and data rates, low latency (typically 1 ms or less), and native support for large machine type communications to deal with the ever increasing demand for wireless services [2]. However, because unallocated conventional microwave bands are scarce, millimeter wave (30-300 GHz) communication has emerged as a promising 5G technology [3]–[7]. The high bandwidth and sparse existing usage are highly attractive advantages. Furthermore, at these frequencies, a large number of antenna elements can be compressed within a small space, which enables massive multiple-input multiple-output (MIMO). Such antenna configurations in turn will potentially reduce out of cell interference, and provide beamforming gains for the desired links. Moreover, millimeter wave standards include IEEE 802.15.3c and IEEE 802.11ad for the 60 GHz band [8]. However, millimeter wave signal propagation is fundamentally different from that in traditional microwave frequencies [9]. Thus, the common adverse effects are high path loss, the sensitivity to blockages, atmospheric absorption, and high noise powers, which will provide significant challenges in utilizing millimeter wave frequencies. For example, the path loss at 60 GHz is 35.6 dB higher than at traditional 1 GHz [10]. Moreover, due to the blockage effects, even the movement of a small object between the transmitter and receiver could cause significant performance losses. Thus, careful design and consideration is required to ensure millimeter wave networks can truly fulfill their potential.

On the other hand, device-to-device (D2D) networks underlaying the cellular networks enable transmissions among close proximity devices for certain applications which saves transmit power and network resources [11]. For example, to provide local access for high rate services, the D2D mode may be the most efficient solution than cellular [12]. Moreover, D2D may act as a relaying service for cell-edge users to connect with a base station in order to improve their signal quality. Thus, enabling D2D mode has also been a key 5G research topic [13], [14], and integrating millimeter wave with D2D is an exciting prospect [12]. However, underlaying D2D below a cellular network provides interference management challenges [15], [16], and the peculiarities of the millimeter wave channel exemplify the challenge of coverage provision. Thus, characterizing the performance of D2D underlaying millimeter-wave cellular is highly important for 5G wireless, and this problem is our main focus within this paper.

A. Related Work

Millimeter-wave cellular research has been extensive recently, mostly utilizing the tools and models from stochastic geometry (study of random point patterns focusing on the theory of spatial point processes). For example, the base station downlink co-operation reduces outage and signifi-

Manuscript received March 23, 2018; revised July 21, 2018 and September 4, 2018; accepted September 4, 2018. Date of publication September 17, 2018; date of current version January 15, 2019. This work was supported in part by Huawei HIRP Project under grant HO2016050002AY. This paper was presented in part at the IEEE International Communications Conference, Paris, France, 2017 [1]. The associate editor coordinating the review of this paper and approving it for publication was D. B. da Costa. *(Corresponding author: Sachitha Kusaladharma.)*

S. Kusaladharma and C. Tellambura are with the Department of Electrical and Computer Engineering, University of Alberta, Edmonton, AB T6G 2R3, Canada (e-mail: kusaladh@ualberta.ca; ct4@ualberta.ca).

Z. Zhang is with the Wireless Technology Cooperation Department, Huawei Technologies Co., Ltd, Shanghai 201206, China (e-mail: zhangzhang4@huawei.com).

Color versions of one or more of the figures in this paper are available online at http://ieeexplore.ieee.org.

Digital Object Identifier 10.1109/TCOMM.2018.2870378

cantly improves the performance in dense networks without small-scale fading [17]. However, for less dense deployment of base stations and for Rayleigh fading, this work also shows that the performance improvement of cooperation is minimal. A general framework for coverage and rate evaluation in millimeter wave networks is proposed in [8] and [18], and dense networks are investigated further in [8] where the line-of-sight region is approximated with a ball. They are found to achieve similar coverage and significantly higher data rates than conventional cellular networks. In contrast, [18] proposes a mathematical framework for the inter-cell interference in ultra-dense deployments. Reference [19] proposes Poisson point process (PPP) based approximations to characterize interference in dynamic time division duplexing and unsynchronized backhaul access. Furthermore, [20] investigates wireless power transfer in a stochastic millimeter wave network by deriving the moment generating function (MGF) and cumulants of the aggregate received power at a typical receiver, while [21] proposes an intensity matching approach for simplified performance results under stochastic models. Reference [22] presents a tractable model for power beacon assisted ad-hoc millimeter wave networks, and provides insights on how system design parameters affect the coverage.

The millimeter wave research has also incorporated D2D networks. For example, [23] analyzes wearable D2D networks within a finite region, and concludes that millimeter bands provide significant throughput gains even with omni-directional antennas. Furthermore [24] proposes an efficient scheduling scheme for millimeter-wave small cells while exploiting D2D links for efficiency. And [25] studies the spatial heterogeneity of outdoor users via the coefficient of variation. The performance of D2D millimeter wave networks is analyzed using the Poisson bipolar model [13]. The meta distribution and approximate signal-to-interference and noise ratio (SINR) are derived along with the mean delay and spatial outage. Moreover, D2D relaying has been proposed to counteract blockages in [26]. The authors develop a model for the downlink coverage probability accounting for beamforming gains, and show that the coverage significantly improves with the use of 2-hop relays. Moreover, [27] proposes a resource allocation scheme for underlaid E-band (60 GHz to 90 GHz) D2D networks and shows that the proposed scheme increases throughput while reducing interference.

B. Motivation and Contribution

In this work, we investigate a D2D network underlaid on a millimeter wave cellular network and characterize the D2D outage. The outage is perhaps the most fundamental and common performance measure of wireless networks, which is simply the probability that SINR falls below the threshold level necessary for guaranteed quality of service. However, D2D outage analysis is complicated due to several factors. First, we need the distribution of the ratio of signal power to interference power. Although the latter is less due to the directionality of the millimeter wave signals, the desired signal power depends on blockages and fading, which are random factors. Second, the received signal powers also depend on log-distance path loss and peak transmit power constraints. Finally, the locations of the users rapidly change due to the mobility of the users, and the locations base stations are also increasingly irregular due to the growth of heterogeneous cellular networks. Consequently, spatial randomness inherent in the overall network is increasing. To accurately identify all these effects, outage analysis must consider stochastic models incorporating spatial randomness.

To this end, we model the locations of the cellular base stations and users as independent homogeneous PPPs [28] and the D2D nodes as a Matérn cluster process in $\mathbb{R}^2$. A Matérn cluster process is an isotropic, stationary Poisson cluster process which consists of parent and offspring points. The latter are located around the parent points and are independently and identically distributed (i.i.d.). Thus, the offspring points are uniformly distributed in a circle centered at each parent. A simplified Boolean blockage model is assumed, and line-of-sight (LOS) and non-line-of-sight (NLOS) conditions are modeled with different log-distance path loss exponents and Nakagami-m parameters. Moreover, we assume directional antenna patterns and perfect antenna beam alignment. These assumptions are standard in the literature. We consider two transmitter-receiver association schemes: (i) each cellular user connects to its nearest base station while a D2D transmitter connects with a random receiver within its cluster (equivalently, each D2D receiver associates with its respective cluster head), (ii) each cellular user connects to the closest LOS base station while a D2D transmitter connects with a random LOS receiver within its cluster. We assume a path loss and antenna gain inversion based power control model where the D2D network is also peak power constrained.

Our main analysis focuses on a D2D link consisting of a D2D transmitter node and a D2D receiver node. Our main contributions of this paper are listed below:

1) we derive the MGF of the interference on the D2D receiver from other D2D transmitters and cellular base stations using stochastic geometry based tools for the nearest association scheme. More precisely, we use the Mapping and Marking theorems relating to Poisson point processes to transform the process of interfering base stations into an equivalent inhomogeneous process which incorporates blockage, antenna gains, transmit power, fading, and path-loss variations.
2) we derive the D2D link outage in closed-form for integer Nakagami-m parameters while considering both the peak power constraints and random blockages for nearest association.
3) we derive D2D link outage and the MGFs of the interference for the LOS association scheme. The distance distributions from the base stations to the users are derived as auxiliary results.

Apart from the outage, the area spectral efficiency [21] and average rate also help to assess system performance and gain valuable insights. However, for the scope of this paper, we focus on the outage, and leave those other performance metrics for future work.

Notations: $\Gamma(x,a) = \int_a^\infty t^{x-1}e^{-t}dt$ and $\Gamma(x) = \Gamma(x,0)$ [29]. $\Pr[A]$ is probability of event A, $f_X(\cdot)$ is

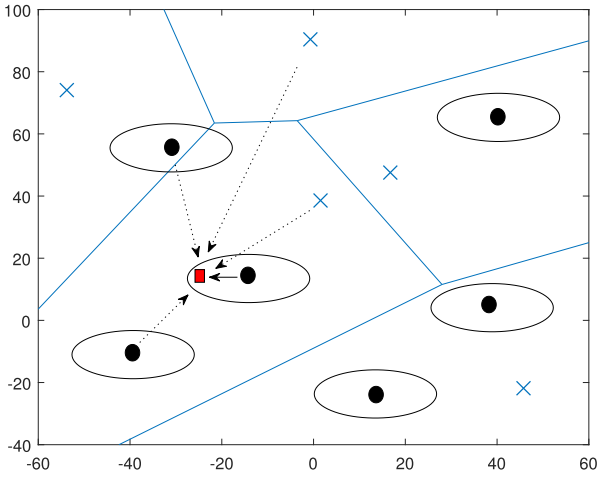

Fig. 1. System model comprises of cellular base stations and D2D clusters in $\mathbb{R}^2$. The blue crosses, black circles and red squares represent the cellular base stations, D2D transmitters. D2D receivers, respectively. Broken arrows and solid arrow represent interference links and desired link, respectively.

probability density function (PDF), $F_X(\cdot)$ is cumulative distribution function (CDF), $M_X(\cdot)$ is the MGF, $M_X^{(k)}(\cdot)$ is the k-th derivative of the MGF, and $\mathbb{E}_X[\cdot]$ denotes the expectation over X.

II. System Model and Assumptions

This section introduces the system parameters and models used throughout the paper.

A. Spatial Distribution and Blockages

We consider four separate types of nodes: 1) cellular base stations, 2) cellular users, 3) D2D transmitters, and 4) D2D receivers. While the D2D transmitters/receivers in principle can also be cellular users, we differentiate them for the ease of analysis. The locations of the cellular base stations and users are modeled as two independent, stationary homogeneous PPPs in $\mathbb{R}^2$ (Fig. 1). The homogeneous PPP has been used widely in the literature to model wireless nodes, and has been shown to be an extremely accurate model [30], [31]. With a homogeneous PPP, the number of nodes within any given area $|\mathcal{A}|$ is given by [32]

$$\Pr[N(|\mathcal{A}|)=n]=\frac{(\lambda|\mathcal{A}|)^n}{n!}e^{-\lambda|\mathcal{A}|}, \tag{1}$$

where λ is the average node density per unit area. Due to the homogeneity, λ is constant and location independent. As such, the cellular-base-station and user processes are respectively denoted as $\Phi_{c,b}$ and $\Phi_{c,u}$ with spatial densities $\lambda_{c,b}$ and $\lambda_{c,u}$, respectively.

The D2D network is modelled as a Matérn cluster process [33]. Within a Matérn cluster process, multiple clusters exist in $\mathbb{R}^2$ where the cluster centers are distributed as a homogeneous Poisson point process and each cluster center is encircled by a daughter process existing within a ball of radius R from it.[1] The daughter processes are homogeneous within their respective annular regions and independent of each other. In our case the cluster centers having a density of $\lambda_{d,t}$ model the D2D transmitters and the daughter nodes having a density of $\lambda_{d,r}$ model the D2D receivers.[2]

Importantly, unlike in the case of sub 6-GHz signals, random objects can block millimeter wave signals reaching the receiver. We will model the blockages stochastically using a rectangular Boolean scheme [34], and the blockages are assumed to be stationary and isotropic. With these assumptions, the probability of a link of length r with no blockage (LOS link) is given by $e^{-\beta r}$, where β is a constant relating to the size and density of the blockages. Similarly, the probability of a NLOS link is given by $1-e^{-\beta r}$. Note that a link is more susceptible to blockage as its length increases. Moreover, for mathematical tractability, we assume that the effect of blockage on different links is independent. Note that the different types of nodes have a chance of falling within the environs of a blocking object. However, although we omit such a scenario, it can be readily incorporated to our analysis through independently thinning the different processes of nodes [8].

B. Channel Model and Antenna Pattern

We assume that the cellular system employs universal frequency reuse [35], and D2D nodes borrow from the same set of cellular frequencies. For mathematical tractability, we assume that the channel gains are independent of the underlying spatial point process of nodes. We include both path loss and small-scale fading for all the links. However, the parameters of these phenomena depend on the LOS or NLOS state of the link.

From the model [36], we write the general path loss for a millimeter wave link of distance r as $PL(r)=c_s r^{\alpha_s}$, where $s\in\{L,N\}$, and L,N correspond to LOS and NLOS links. The parameter α_s is the path loss exponent while c_s is the intercept. The small-scale fading is assumed to be Nakagami-m. Thus, the channel fading power gain ($|h_s|^2$) is distributed as [37], [38]

$$f_{|h_s|^2}(x)=\frac{m_s^{m_s}}{\Gamma(m_s)}x^{m_s-1}e^{-m_s x},\quad 0\le x<\infty,\ m\in[0.5,\infty), \tag{2}$$

where the Nakagami parameter $m_s(s\in\{L,N\})$ indicates the degree of fading severity. For instance, $m_s\to\infty$ indicates a lack of fading while $m_s=1$ indicates Rayleigh fading. In millimeter wave LOS links, the number of scatterers is relatively few. Thus, the LOS link fading is less severe, which is modeled by relatively large m_L. Conversely, the NLOS parameter m_N is smaller. It should be noted that accurate cluster-based channel models such as the Saleh-Valenzuela model [39]–[41] are mathematically intractable. Thus, we omit such models in this work.

In millimeter bands, highly dense packing of antenna elements enables directional beamforming. We thus assume directional beamforming for all our transmit and receive nodes. Moreover, the antenna gain patterns of cellular users and D2D transmitters/receivers are identical while cellular base stations

[1]Note that this system model is analogous to a homogeneous Poisson point process of D2D receivers where the transmitters only select a receiver within a given radius.

[2]We assume that each daughter process has the same constant density.

have a different pattern. For a concise analysis, we consider a sectored antenna model [35] where the antenna gain pattern is divided into discrete regions based on the angle off the boresight direction. Thus, the antenna gain ($G_*(* \in \{cb, u\})$ where cb and u respectively denote cellular base stations and all other types of nodes) can be expressed as follows:

$$G_* = \begin{cases} M_*, & |\theta| \leq \dfrac{\omega_*}{2} \\ m_*, & \text{otherwise,} \end{cases} \tag{3}$$

where ω_* is the antenna beamwidth, θ is the angle off the boresight direction, M_* is the main lobe gain, and m_* is the gain from the side and back lobes. While this gain pattern can be generalized for different side and back lobe gains, and angle dependent main lobe gains, we defer it for future work. The beamforming pattern itself could be based on digital beamforming, analog beamforming, or hybrid beamforming, and is beyond the scope of our paper.

Both cellular and D2D transmitters and receivers perform a beam sweeping process initially in order to estimate the angle of arrival, and we assume that perfect estimation takes place [35]. As such, the combined antenna gains of intended cellular and D2D links are $M_{cb}M_u$ and M_u^2 respectively. The gains of all other links vary randomly depending on the angle off boresight. Note that antenna beam misalignment can also be a significant issue, but it is beyond the scope of this paper.

C. Power Control

We make several standard assumptions about power control. Thus, all transmit nodes (both cellular and D2D) perfectly invert both path loss and antenna gains to reach a receiver at distance r. Thus, the necessary transmit power becomes $P_T = \frac{\rho c_s r^{\alpha_s}}{M_* M_u}$, where $s \in \{L, N\}$, $* \in \{cb, u\}$, and ρ (receiver sensitivity) is the minimum level of power needed by a receiver node for satisfactory performance. For brevity, we assume the same receiver sensitivity ρ for both cellular and D2D receivers, but different sensitivities can be readily incorporated if needed. Furthermore, we assume that the D2D transmit nodes are peak power constrained, which is typical for many practical wireless systems due to regulatory constraints and technical issues. The peak constraint forces the node to abort transmission if the necessary power level exceeds the constraint. For instance, if P_{d2d} is the peak transmit power allowed, a D2D node will abort transmission whenever $P_T > P_{d2d}$.

III. Nearest Association

We assume each cellular user connects to its closest base station. Generally, the closest base station provides the best transmitter-receiver link in terms of the average received signal power, and this base station also has the highest probability of being LOS from the receiver (however, this base station could still be NLOS, which is a drawback, which motivates the LOS association model of the next section). Moreover, this association is the least complicated association strategy for a user especially if prior location information is known. This and other association policies have been studied extensively [42] where the serving BS may be selected on the basis of (a) received signal quality and/or (b) cell traffic load. However, those schemes may have the cost of added complexity and processing power.

In this paper, we assume at most a single associated cellular user for each base station within a given time-frequency block. Then, if the distance between the i-th cellular base station $\phi_{c,b}^i \in \Phi_{c,b}$ and its associated receiver $\phi_{c,u}^i \in \Phi_{c,u}$ is r_c, then it is Rayleigh distributed [43]:

$$f_{r_c}(x) = 2\pi\lambda_{c,b} x e^{-\pi\lambda_{c,b}x^2}, \quad 0 < x < \infty. \tag{4}$$

In the D2D network, each receiver associates with the corresponding transmitter within its cluster. It should be noted that because clusters overlap, a receiver may find a transmitter other than its own cluster head to be the closest. However, receivers are assumed to connect to the transmitter within its own cluster, and thus are only allowed to associate within the cluster [15].

Thus, the distribution of the link distance r_{d2d} can be expressed as [43]

$$f_{r_{d2d}}(x) = \frac{2x}{R^2}, \quad 0 < x < R. \tag{5}$$

A. Outage Performance

We consider a typical D2D receiver and its transmitter with the link distance of r_{d2d} (desired D2D link in Fig. 1). Without the loss of generality, we assume that the D2D receiver is located at the origin. The outage probability (P_O) is defined as $P_O = \Pr[\gamma < \gamma_{th}]$, where γ and γ_{th} are the SINR and the SINR reception threshold of the receiver. The SINR can be written as

$$\gamma = \frac{P_s |h_s|^2 M_u^2 c_s^{-1} r_{d2d}^{-\alpha_s}}{I_c + I_{d2d} + N}, \tag{6}$$

where P_s is the transmit power, I_c is the interference from cellular base stations, I_{d2d} is the interference from other D2D transmitters, and N is the noise power. Note that γ depends on the link being in LOS or NLOS states. Moreover, P_s is a random variable depending on the power control, which in turn depends on the transmitter-receiver distance, LOS/NLOS nature of the link, and the peak power level.

We can use the law of total probability to express P_O as

$$\begin{aligned} P_O &= \mathbb{E}[a_l P_{O,L} + a_N P_{O,N}] \\ &= \frac{2P_{O,L}}{\beta^2 R^2}\left(1 - e^{-\beta R}(\beta R + 1)\right) \\ &\quad + P_{O,N}\left(1 - \frac{2}{\beta^2 R^2}\left(1 - e^{-\beta R}(\beta R + 1)\right)\right), \end{aligned} \tag{7}$$

where $a_L = e^{-\beta r_{d2d}}$ and $a_N = 1 - e^{-\beta r_{d2d}}$ denote the probability of LOS or NLOS link, respectively, while $P_{O,L}$ and $P_{O,N}$ are respectively the conditional outages given LOS and NLOS links. While the pairs of $P_{O,L}$, a_L and $P_{O,N}$, a_N are correlated in general, the correlation disappears for the specific path loss inversion based power control scheme used. Thus, a decoupling of the two terms can be performed.

1) Deriving $P_{O,L}$: When a LOS link exists between the D2D transmitter and receiver given link distance r_{d2d}, we can express $P_{O,L}$ as (See appendix A for proof)

$$\begin{aligned} P_{O,L} = 1 - \tau_L e^{-\frac{m_L \gamma_{th} N}{\rho}} \sum_{\nu=0}^{m_L-1} \frac{1}{\nu!} \left(\frac{m_L \gamma_{th}}{\rho}\right)^{\nu} \sum_{\mu=0}^{\nu} \binom{\nu}{\mu} \\ \times N^{\nu-\mu} \sum_{\kappa=0}^{\mu} \binom{\mu}{\kappa} \\ \times (-1)^{\kappa} M_{I_c}^{(\kappa)} \left(s|_{s=\frac{m_L \gamma_{th}}{\rho}}\right) (-1)^{\mu-\kappa} M_{I_{d2d}}^{(\mu-\kappa)} \\ \times \left(s|_{s=\frac{m_L \gamma_{th}}{\rho}}\right), \end{aligned} \tag{8}$$

where τ_L is written as

$$\tau_L = \begin{cases} \frac{1}{R^2} \left(\frac{P_{d2d} M_u^2}{\rho c_L}\right)^{\frac{2}{\alpha_L}}, & \text{if } \left(\frac{P_{d2d} M_u^2}{\rho c_L}\right)^{\frac{1}{\alpha_L}} < R \\ 1, & \text{if } \left(\frac{P_{d2d} M_u^2}{\rho c_L}\right)^{\frac{1}{\alpha_L}} > R. \end{cases} \tag{9}$$

2) Deriving $P_{O,N}$: In a similar way to $P_{O,L}$, $P_{O,N}$ can be derived as

$$\begin{aligned} P_{O,N} = 1 - \tau_N e^{-\frac{m_N \gamma_{th} N}{\rho}} \sum_{\nu=0}^{m_N-1} \frac{1}{\nu!} \left(\frac{m_N \gamma_{th}}{\rho}\right)^{\nu} \\ \times \sum_{\mu=0}^{\nu} \binom{\nu}{\mu} N^{\nu-\mu} \sum_{\kappa=0}^{\mu} \binom{\mu}{\kappa} (-1)^{\kappa} M_{I_c}^{(\kappa)} \left(s|_{s=\frac{m_N \gamma_{th}}{\rho}}\right) \\ \times (-1)^{\mu-\kappa} M_{I_{d2d}}^{(\mu-\kappa)} \left(s|_{s=\frac{m_N \gamma_{th}}{\rho}}\right), \end{aligned} \tag{10}$$

where τ_N is given by

$$\tau_N = \begin{cases} \frac{1}{R^2} \left(\frac{P_{d2d} M_u^2}{\rho c_N}\right)^{\frac{2}{\alpha_N}}, & \text{if } \left(\frac{P_{d2d} M_u^2}{\rho c_N}\right)^{\frac{1}{\alpha_N}} < R \\ 1, & \text{if } \left(\frac{P_{d2d} M_u^2}{\rho c_N}\right)^{\frac{1}{\alpha_N}} > R. \end{cases} \tag{11}$$

It should be noted that the expressions for $P_{O,L}$ and $P_{O,N}$ are valid for integer Nakagami-m parameters. For non-integer values, numerical techniques must be applied.

B. Interference Statistics

The probability distribution of the aggregate interference is generally intractable. However, since it is the sum of multiple interference terms, an MGF based approach may be more tractable for analysis [37], [43]–[48]. The reason is that the MGF of the aggregate interference is the product of MGFS of individual summands (if independent) [44], [48].

Thus, we next derive the MGFs of the interference powers from both cellular and other D2D transmitters M_{I_c} and $M_{I_{d2d}}$. We assume that all transmitters/base stations (of cellular and D2D) are always active. This assumption is justifiable because the spatial density of transmitter nodes is significantly lower than that of the relevant receivers. Moreover, some random base stations/transmitters are non-active, then the concept independent thinning of point processes can be used to make the necessary adjustments.

The interference from cellular base stations I_c can be divided into two separate terms composed of LOS and

$$\begin{aligned} \mathbb{U}_{c,L} = \frac{\rho^{\frac{2+k}{\alpha_L}} \Gamma\left(m_L + \frac{2+k}{\alpha_L}\right)}{4\pi^2 \Gamma(m_L) m_L^{-\frac{2+k}{\alpha_L}} (M_u M_{cb})^{\frac{2+k}{\alpha_L}}} \left(\theta_{cb} M_{cb}^{\frac{2+k}{\alpha_L}} + (2\pi - \theta_{cb}) m_{cb}^{\frac{2+k}{\alpha_L}}\right) \left(\theta_u M_u^{\frac{2+k}{\alpha_L}} + (2\pi - \theta_u) m_u^{\frac{2+k}{\alpha_L}}\right) \\ \times \left(\frac{c_L^{\frac{2+k}{\alpha_L}}}{(\pi \lambda_{c,b})^{\frac{3+k}{2}}} \left(\sqrt{\pi \lambda_{c,b}} \Gamma\left(\frac{k+2}{2}\right) \, {}_1\mathcal{F}_1\left(\frac{k+2}{2}; \frac{1}{2}; \frac{\beta^2}{4\pi\lambda_{c,b}}\right) - \beta \Gamma\left(\frac{k+5}{2}\right) \, {}_1\mathcal{F}_1\left(\frac{k+5}{2}; \frac{3}{2}; \frac{\beta^2}{4\pi\lambda_{c,b}}\right)\right) \right. \\ + \frac{c_N^{\frac{2+k}{\alpha_L}}}{(\pi\lambda_{c,b})^{\frac{\alpha_L + \alpha_N(2+k)}{2\alpha_L}}} \left(-\sqrt{\pi\lambda_{c,b}} \Gamma\left(1 + \frac{(2+k)\alpha_N}{2\alpha_L}\right) \left(\, {}_1\mathcal{F}_1\left(1 + \frac{(2+k)\alpha_N}{2\alpha_L}; \frac{1}{2}; \frac{\beta^2}{4\pi\lambda_{c,b}}\right) - 1\right) \right. \\ \left. \left. + \beta \Gamma\left(\frac{3}{2} + \frac{(2+k)\alpha_N}{2\alpha_L}\right) \, {}_1\mathcal{F}_1\left(\frac{3}{2} + \frac{(2+k)\alpha_N}{2\alpha_L}; \frac{3}{2}; \frac{\beta^2}{4\pi\lambda_{c,b}}\right)\right)\right) \end{aligned} \tag{12}$$

$$\begin{aligned} \mathbb{U}_{c,N} = \frac{\rho^{\frac{2+k}{\alpha_N}} \Gamma\left(m_N + \frac{2+k}{\alpha_N}\right)}{4\pi^2 \Gamma(m_N) m_N^{-\frac{2+k}{\alpha_N}} (M_u M_{cb})^{\frac{2+k}{\alpha_N}}} \left(\theta_{cb} M_{cb}^{\frac{2+k}{\alpha_N}} + (2\pi - \theta_{cb}) m_{cb}^{\frac{2+k}{\alpha_N}}\right) \left(\theta_u M_u^{\frac{2+k}{\alpha_N}} + (2\pi - \theta_u) m_u^{\frac{2+k}{\alpha_N}}\right) \\ \times \left(\frac{c_L^{\frac{2+k}{\alpha_N}}}{(\pi \lambda_{c,b})^{\frac{\alpha_N + \alpha_L(2+k)}{\alpha_N}}} \left(\sqrt{\pi \lambda_{c,b}} \Gamma\left(\frac{(k+2)\alpha_L}{2\alpha_N}\right) \, {}_1\mathcal{F}_1\left(\frac{(k+2)\alpha_L}{2\alpha_N}; \frac{1}{2}; \frac{\beta^2}{4\pi\lambda_{c,b}}\right) \right. \right. \\ \left. - \beta \Gamma\left(\frac{3}{2} + \frac{(2+k)\alpha_L}{2\alpha_N}\right) \, {}_1\mathcal{F}_1\left(\frac{3}{2} + \frac{(2+k)\alpha_L}{2\alpha_N}; \frac{3}{2}; \frac{\beta^2}{4\pi\lambda_{c,b}}\right)\right) \\ + \frac{c_N^{\frac{2+k}{\alpha_N}}}{(\pi\lambda_{c,b})^{\frac{3+k}{2}}} \left(-\sqrt{\pi\lambda_{c,b}} \Gamma\left(1 + \frac{2+k}{2}\right) \left(\, {}_1\mathcal{F}_1\left(1 + \frac{2+k}{2}; \frac{1}{2}; \frac{\beta^2}{4\pi\lambda_{c,b}}\right) - 1\right) \right. \\ \left. \left. + \beta \Gamma\left(\frac{k+5}{2}\right) \, {}_1\mathcal{F}_1\left(\frac{k+5}{2}; \frac{3}{2}; \frac{\beta^2}{4\pi\lambda_{c,b}}\right)\right)\right) \end{aligned} \tag{13}$$

NLOS cellular base stations using the thinning property [49]. If $I_{c,L}$ and $I_{c,N}$ denote these two terms, $I_c = I_{c,L} + I_{c,N}$. Moreover, $M_{I_c} = M_{I_{c,L}} M_{I_{c,N}}$ due to the independence of thinned Poisson point processes [49].

1) Deriving $M_{I_{c,L}}$: The expression for $M_{I_{c,L}}$ is derived as (see Appendix B for proof)

$$M_{I_{c,L}} = e^{\left(\int_0^\infty \left(e^{-s(c_L r)^{-1}} - 1\right)\bar{\lambda}_{c,bL}\, dr\right)} = e^{\sum_{k=0}^{\infty} \frac{2\pi\lambda_{c,b}(-\beta)^k}{\alpha_L k!}\left(\frac{s}{c_L}\right)^{\frac{2+k}{\alpha_L}}\Gamma\left(-\frac{2+k}{\alpha_L}\right)\mathbb{U}_{c,L}}. \quad (14)$$

2) Deriving $M_{I_{c,N}}$: Using similar arguments as with the derivation of $M_{I_{c,L}}$, $M_{I_{c,N}}$ ca be written as

$$M_{I_{c,N}} = e^{\sum_{k=1}^{\infty} -\frac{2\pi\lambda_{c,b}(-\beta)^k}{\alpha_N k!}\left(\frac{s}{c_N}\right)^{\frac{2+k}{\alpha_N}}\Gamma\left(-\frac{2+k}{\alpha_N}\right)\mathbb{U}_{c,N}}, \quad (15)$$

where $\mathbb{U}_{c,N}$ is given in (13), as shown at the bottom of the previous page.

The interference from other D2D transmitters on the D2D receiver in question can be decomposed into LOS ($I_{d2d,L}$) and NLOS ($I_{d2d,N}$) components with $I_{d2d} = I_{d2d,L} + I_{d2d,N}$ and $M_{I_{d2d}} = M_{I_{d2d,L}} M_{I_{d2d,N}}$.

3) MGF pf $I_{d2d,L}$: While the derivation of $M_{I_{d2d,L}}$ is similar to $M_{I_{c,L}}$ and $M_{I_{c,N}}$, a complication arises while obtaining the $\frac{2+k}{\alpha}$-th moment of the transmit power of a D2D transmitter (P_{dL}). If r_d is the distance from a D2D transmitter to the associated receiver, P_{dL} takes $\frac{\rho c_L r_d^{\alpha_L}}{M_u^2}$ with probability $e^{-\beta r_d}\tau_L$, $\frac{\rho c_N r_d^{\alpha_N}}{M_u^2}$ with probability $(1-e^{-\beta r_d})\tau_N$, and 0 with probability $e^{-\beta r_d}(1-\tau_L)+(1-e^{-\beta r_d})(1-\tau_N)$ after considering blockages and peak power constraints. Moreover, while τ_L (35) and τ_N (11) can take multiple combinations as evident from their expressions, we consider the case where $\max\left(\left(\frac{P_{d2d}M_u^2}{\rho c_N}\right)^{\frac{1}{\alpha_N}}, \left(\frac{P_{d2d}M_u^2}{\rho c_L}\right)^{\frac{1}{\alpha_L}}\right) < R$ for this paper.

After using the Slivnyak's theorem [49] to remove the desired transmitter from the field of interferers, $M_{I_{d2d,L}}$ is expressed as

$$M_{I_{d2d,L}} = e^{\sum_{k=0}^{\infty} \frac{2\pi\lambda_{d,t}(-\beta)^k}{\alpha_L k!}\left(\frac{s}{c_L}\right)^{\frac{2+k}{\alpha_L}}\Gamma\left(-\frac{2+k}{\alpha_L}\right)\mathbb{U}_{d,L}}, \quad (16)$$

where $\mathbb{U}_{d,L}$ and $\mathbb{U}_{d,N}$ are given in (18) and (19), respectively, as shown at the bottom of this page.

4) Deriving $M_{I_{d2d,N}}$: The expression for $M_{I_{d2d,N}}$ is obtained as

$$M_{I_{d2d,N}} = e^{\sum_{k=1}^{\infty} -\frac{2\pi\lambda_{d,t}(-\beta)^k}{\alpha_N k!}\left(\frac{s}{c_N}\right)^{\frac{2+k}{\alpha_N}}\Gamma\left(-\frac{2+k}{\alpha_N}\right)\mathbb{U}_{d,N}}. \quad (17)$$

IV. LOS Association

While the previous section considered the closest transmitter association, this may not be the best if this link is NLOS, which will result in outages or increased power at the transmitters in order to compensate for the adverse channel. This motivates us to consider LOS association in this section, where an association occurs only if the transmitter-receiver link is LOS. In this case, both cellular and D2D receivers associate with closest LOS base station and D2D transmitter within a radius of R, respectively. Due to this, the distribution of the cellular base station and receiver distance r_c and the D2D transmitter receiver distance r_{d2d} do not follow (4) and (5).

When LOS association takes place, the PDFs of r_c and r_{d2d} can be respectively written as (see Appendix C and

$$\mathbb{U}_{d,L} = \frac{1}{2\pi^2 R^2}\left(\frac{\rho}{M_u^2}\right)^{\frac{2+k}{\alpha_L}} \frac{\Gamma\left(m_L + \frac{2+k}{\alpha_L}\right)}{\Gamma(m_L) m_L^{-\frac{2+k}{\alpha_L}}} \left(\theta_u M_u^{\frac{2+k}{\alpha_L}} + (2\pi-\theta_u) m_u^{\frac{2+k}{\alpha_L}}\right)^2 \times \left(\frac{c_L^{\frac{2+k}{\alpha_L}}}{\beta^{4+k}}\left(\Gamma(4+k) - \Gamma\left(4+k, \beta\left(\frac{P_{d2d}M_u^2}{c_L\rho}\right)^{\frac{1}{\alpha_L}}\right)\right)\right. + \frac{c_N^{\frac{2+k}{\alpha_L}}}{(2\alpha_L+(2+k)\alpha_N)\beta^{\frac{2\alpha_L+(2+k)\alpha_N}{\alpha_L}}}\left(\alpha_L\left(\beta\left(\frac{P_{d2d}M_u^2}{c_N\rho}\right)^{\frac{1}{\alpha_N}}\right)^{\frac{2\alpha_L+(2+k)\alpha_N}{\alpha_L}}\right. \left.\left. - (2\alpha_L+(2+k)\alpha_N)\left(\Gamma\left(\frac{2\alpha_L+(2+k)\alpha_N}{\alpha_L}\right) - \Gamma\left(\frac{2\alpha_L+(2+k)\alpha_N}{\alpha_L}, \beta\left(\frac{P_{d2d}M_u^2}{c_N\rho}\right)^{\frac{1}{\alpha_N}}\right)\right)\right)\right) \quad (18)$$

$$\mathbb{U}_{d,N} = \frac{1}{2\pi^2 R^2}\left(\frac{\rho}{M_u^2}\right)^{\frac{2+k}{\alpha_N}} \frac{\Gamma\left(m_N + \frac{2+k}{\alpha_N}\right)}{\Gamma(m_N) m_N^{-\frac{2+k}{\alpha_N}}} \left(\theta_u M_u^{\frac{2+k}{\alpha_N}} + (2\pi-\theta_u) m_u^{\frac{2+k}{\alpha_N}}\right)^2 \times \left(\frac{c_L^{\frac{2+k}{\alpha_N}}}{\beta^{\frac{2\alpha_N+(2+k)\alpha_L}{\alpha_N}}}\left(\Gamma\left(\frac{2\alpha_N+(2+k)\alpha_L}{\alpha_N}\right) - \Gamma\left(\frac{2\alpha_N+(2+k)\alpha_L}{\alpha_N}, \beta\left(\frac{P_{d2d}M_u^2}{c_L\rho}\right)^{\frac{1}{\alpha_L}}\right)\right)\right. + \frac{c_N^{\frac{2+k}{\alpha_N}}}{(4+k)\beta^{4+k}}\left(\left(\beta\left(\frac{P_{d2d}M_u^2}{c_N\rho}\right)^{\frac{1}{\alpha_N}}\right)^{4+k} - (4+k)\left(\Gamma(4+k) - \Gamma\left(4+k, \beta\left(\frac{P_{d2d}M_u^2}{c_N\rho}\right)^{\frac{1}{\alpha_N}}\right)\right)\right)\right) \quad (19)$$

Appendix D for proof)

$$f_{r_c}(x) = 2\pi\lambda_{c,b} x e^{-\frac{2\pi\lambda_{c,b}}{\beta^2}(1-e^{-\beta x}(\beta x+1))-\beta x}, \quad 0 < x < \infty, \tag{20}$$

and

$$f_{r_{d2d}}(x) = \frac{\beta^2 x e^{-\beta x}}{1-e^{-\beta R}(\beta R+1)}, \quad 0 < x < R. \tag{21}$$

A. Outage Performance

Similar to the previous section, our objective is to find the outage performance of a typical D2D receiver located at the origin. Thus, we can write the outage probability P_O as

$$P_O = \Pr\left[\frac{P_L |h_L|^2 M_u^2 c_L^{-1} r_{d2d}^{-\alpha_L}}{I_c + I_{d2d} + N} < \gamma_{th}\right], \tag{22}$$

where the transmit power P_L is equivalent to (34). If τ_L is the probability that $P_L = \frac{\rho c_L r_{d2d}^{\alpha_L}}{M_u^2}$, it can be expressed as

$$\begin{aligned}\tau_L &= \Pr\left[r_{d2d} < \left(\frac{P_{d2d} M_u^2}{\rho c_L}\right)^{\frac{1}{\alpha_L}}\right] \\ &= \begin{cases} \dfrac{1-e^{-\beta\xi}(\beta\xi+1)}{1-e^{-\beta R}(\beta R+1)}, & \text{if } \xi < R \\ 1, & \text{if } \xi > R. \end{cases}\end{aligned} \tag{23}$$

where $\xi = \left(\frac{P_{d2d} M_u^2}{\rho c_L}\right)^{\frac{1}{\alpha_L}}$. The expression for P_O in (22) can be simplified in an identical manner to the derivation of $P_{O,L}$ in Section III. As such, the final expression for P_O is identical to (36) with τ being given in (23).

B. Interference Characteristics

We will now characterize the interference from cellular and other D2D transmitters (I_{d2d} and Ic) in terms of the MGF. Similar to the previous section both the interference terms can be divided into two terms depending on whether the interfering transmitter is LOS or not to the D2D receiver in question. Thus, $M_{I_c} = M_{I_{c,L}} M_{I_{c,N}}$ and $M_{I_{d2d}} = M_{I_{d2d,L}} M_{I_{d2d,N}}$.

In deriving these terms, we employ the same mapping procedure as Section III, and obtain equivalent distributions for the relevant interfering nodes. For example, the distribution of LOS cellular interferers has the intensity (39). However, while the expressions for $\mathbb{E}\left[(|h_{cL}|^2)^{\frac{2+k}{\alpha_L}}\right]$ and $\mathbb{E}\left[P_{cL}^{\frac{2+k}{\alpha_L}}\right]$ remain the same as in Section III, $\mathbb{E}\left[P_{cL}^{\frac{2+k}{\alpha_L}}\right]$ changes due to the different association procedure. P_{cL} is given by

$$P_{cL} = \frac{\rho c_L r_c^{\alpha_L}}{M_U M_{cb}}. \tag{24}$$

As such, we can write

$$\begin{aligned}&\mathbb{E}\left[P_{cL}^{\frac{2+k}{\alpha_L}}\right] \\ &= \left(\frac{\rho c_L}{M_U M_{cb}}\right)^{\frac{2+k}{\alpha_L}} \\ &\quad \times \int_{x=0}^{\infty} 2\pi\lambda_{c,b} x^{3+k} e^{-\frac{2\pi\lambda_{c,b}}{\beta^2}(1-e^{-\beta x}(\beta x+1))-\beta x} dx.\end{aligned} \tag{25}$$

With this knowledge, $M_{I_{c,L}}$ is obtained in a similar manner to (44) as

$$M_{I_{c,L}} = e^{\sum_{k=0}^{\infty} \frac{2\pi\lambda_{c,b}(-\beta)^k}{\alpha_L k!}\left(\frac{s}{c_L}\right)^{\frac{2+k}{\alpha_L}}\Gamma\left(-\frac{2+k}{\alpha_L}\right)\mathbb{V}_{c,L}}, \tag{26}$$

where $\mathbb{V}_{c,L}$ is given by (29), as shown at the bottom of the next page.

Using similar arguments, $M_{I_{c,N}}$ can be obtained as

$$M_{I_{c,N}} = e^{\sum_{k=1}^{\infty} -\frac{2\pi\lambda_{c,b}(-\beta)^k}{\alpha_N k!}\left(\frac{s}{c_N}\right)^{\frac{2+k}{\alpha_N}}\Gamma\left(-\frac{2+k}{\alpha_N}\right)\mathbb{V}_{c,N}}, \tag{27}$$

where $\mathbb{V}_{c,N}$ is given by (30), as shown at the bottom of the next page.

We now must derive the MGFs from LOS and NLOS active D2D transmitters. However, due to peak power constraints, not all D2D transmitters are active. It was shown that each D2D transmitter has a probability of transmission given by τ_L (23). Using independent thinning [49], the intensity of active D2D transmitters becomes $\tau_L \lambda_{d,t}$. Therefore, using similar arguments as the derivation of $M_{I_{c,L}}$, and under the assumption that $\left(\frac{P_{d2d} M_u^2}{\rho c_L}\right)^{\frac{1}{\alpha_L}} < R$, we can express $M_{I_{d2d,L}}$ and $M_{I_{d2d,N}}$ as

$$\begin{aligned}M_{I_{d2d,L}} &= e^{\sum_{k=0}^{\infty} \frac{2\pi\tau_L\lambda_{d,t}(-\beta)^k}{\alpha_L k!}\left(\frac{s}{c_L}\right)^{\frac{2+k}{\alpha_L}}\Gamma\left(-\frac{2+k}{\alpha_L}\right)\mathbb{V}_{d2d,L}} \\ M_{I_{d2d,N}} &= e^{\sum_{k=1}^{\infty} -\frac{2\pi\tau_L\lambda_{d,t}(-\beta)^k}{\alpha_N k!}\left(\frac{s}{c_N}\right)^{\frac{2+k}{\alpha_N}}\Gamma\left(-\frac{2+k}{\alpha_N}\right)\mathbb{V}_{d2d,N}},\end{aligned} \tag{28}$$

where $\mathbb{V}_{d2d,L}$ and $\mathbb{V}_{d2d,N}$ are respectively given in (31) and (32), as shown at the bottom of the next page.

V. Numerical Results

We next present performance trends of millimeter wave D2D networks for several system parameter configurations. The details of the simulation setup are as follows. A 100MHz bandwidth is considered (with a resultant noise power of -94 dBm) in the 28 GHz band along with intercepts $cL = cN = 10^5$, and path loss exponents $\alpha_L = 2.1$ and $\alpha_N = 4.1$. Moreover, unless stated otherwise, $\lambda_{c,b} = 10^{-4}$, $\theta_c = \theta_u = \frac{\pi}{10}$, $M_c = 20$ dB, $m_c = m_u = -10$ dB, $\rho = -80$ dBm, and $\beta = 0.001$.

We first investigate the performance of nearest association. Fig. 2 plots the outage as a function of the SINR threshold γ_{th}. It is clear that D2D operation is infeasible when $\gamma_{th} > -20$ dB. Such high outage levels arise due to four major factors affecting the D2D receiver: interference from cellular base stations, interference from other D2D transmitters, thermal noise due to the high bandwidth, and the outage due to the associated transmitter being cut-off due to the peak power constraint. When $M_u = 10$ dB, increasing the cluster radius R generally increases outage. This is due to two reasons. First, a higher radius causes other D2D transmitters to transmit at a higher power level, increasing interference. This effect is amplified due to the fact that the probability of a NLOS link increases with the cell radius. Second, as the cell radius increases, the desired link itself has an increased tendency to be NLOS, resulting in more severe fading and being cut-off

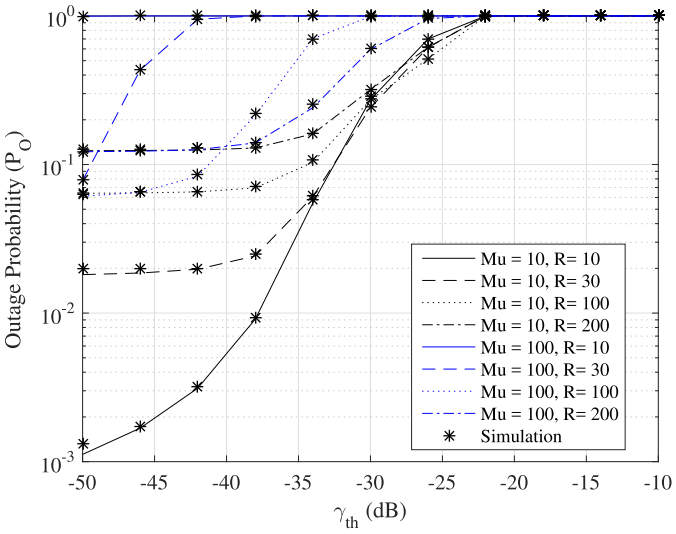

Fig. 2. The outage probability (P_O) vs. γ_{th} in dB for nearest association with different D2D cell radii (R) and M_u. $\lambda_{d,t} = 10^{-4}$, $m_L = 4$, $m_N = 2$, and $P_{d2d} = -10$ dBm.

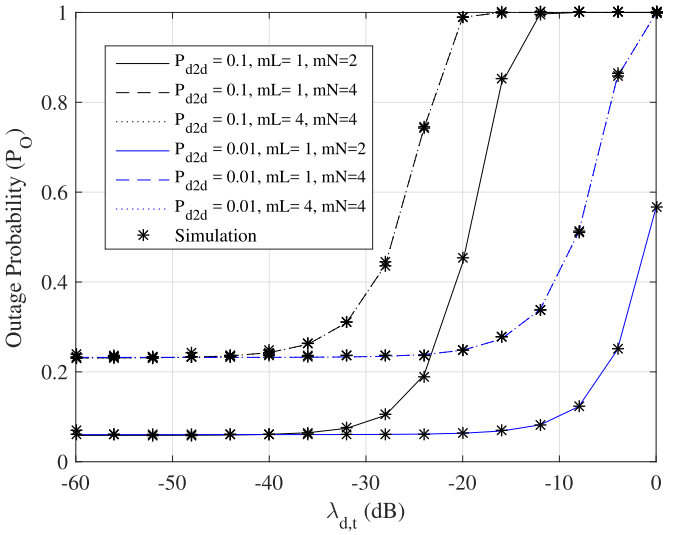

Fig. 3. The outage probability (P_O) vs. the D2D transmitter density $\lambda_{d,t}$ in dB for nearest association under varying m_L, m_N, and P_{d2d}. $\gamma_{th} = 10^{-3}$, $R = 20$, and $M_u = 10$ dB.

due to the required power exceeding the peak power threshold. However, when M_u is increased to 20 dB, the trend is unclear. As R is increased, the outage roughly drops and then increases again. This is due to two competing effects occurring for a M_u value; the desired link would have a lower probability to get cut-off due to the lower transmit power needed, and the intra-D2D interference increases because a lesser number of interfering D2D transmitters get cut-off. At a certain radius, the effect of the latter outweighs the former, and the outage increases. Moreover, it is important to note that the R and M_u pair providing the best performance also depends on the specific SINR threshold γ_{th}.

The outage probability is plotted against the D2D transmitter density $\lambda_{d,t}$ in Fig. 3. While a higher $\lambda_{d,t}$ causes the outage to approach 1 due to intra-D2D interference, reducing $\lambda_{d,t}$ causes the outage to first drop abruptly, and then flatten out towards a value determined by noise and inter-network interference. Interestingly, note that the outage probability increases when m_L is increased from 2 to 4. While this may seem counter-intuitive, it is because the intra-D2D interference being less severely faded. However, the change in the outage when m_N changes is negligible, and the curves for $m_N = 1$ and $m_N = 2$ almost overlap. Moreover, it is interesting to note that while a lower P_{d2d} provides a lower outage at very low $\lambda_{d,t}$ values, the converse is true when $\lambda_{d,t}$ increases. As P_{d2d} is lower, more D2D transmitters requiring additional power to transmit due to the increased radius get cut-off; thus reducing interference. However, under this scenario, the desired link also has an increased cut-off probability, which becomes more prominent when $\lambda_{d,t}$ is lower.

$$\mathbb{V}_{c,L} = \frac{\lambda_{c,b}}{2\pi}\left(\theta_{cb}M_{cb}^{\frac{2+k}{\alpha_L}} + (2\pi-\theta_{cb})m_{cb}^{\frac{2+k}{\alpha_L}}\right)\left(\theta_u M_u^{\frac{2+k}{\alpha_L}} + (2\pi-\theta_u)m_u^{\frac{2+k}{\alpha_L}}\right) \times \frac{\Gamma\left(m_L+\frac{2+k}{\alpha_L}\right)}{\Gamma(m_L)}\left(\frac{\rho m_L c_L}{M_U M_{cb}}\right)^{\frac{2+k}{\alpha_L}} \int_{x=0}^{\infty} x^{3+k} e^{-\frac{2\pi\lambda_{c,b}}{\beta^2}(1-e^{-\beta x}(\beta x+1))-\beta x} dx \tag{29}$$

$$\mathbb{V}_{c,N} = \frac{\lambda_{c,b}}{2\pi}\left(\theta_{cb}M_{cb}^{\frac{2+k}{\alpha_N}} + (2\pi-\theta_{cb})m_{cb}^{\frac{2+k}{\alpha_N}}\right)\left(\theta_u M_u^{\frac{2+k}{\alpha_N}} + (2\pi-\theta_u)m_u^{\frac{2+k}{\alpha_N}}\right) \times \frac{\Gamma\left(m_N+\frac{2+k}{\alpha_N}\right)}{\Gamma(m_N)}\left(\frac{\rho m_N c_L}{M_U M_{cb}}\right)^{\frac{2+k}{\alpha_N}} \int_{x=0}^{\infty} x^{1+\frac{\alpha_L(2+k)}{\alpha_N}} e^{-\frac{2\pi\lambda_{c,b}}{\beta^2}(1-e^{-\beta x}(\beta x+1))-\beta x} dx \tag{30}$$

$$\mathbb{V}_{d2d,L} = \frac{1}{4\pi^2\tau_L}\left(\theta_u M_u^{\frac{2+k}{\alpha_L}} + (2\pi-\theta_u)m_u^{\frac{2+k}{\alpha_L}}\right)^2 \frac{\Gamma\left(m_L+\frac{2+k}{\alpha_L}\right)}{\Gamma(m_L)}\left(\frac{\rho m_L c_L}{M_u^2}\right)^{\frac{2+k}{\alpha_L}} \int_{x=0}^{\left(\frac{P_{d2d}M_u^2}{\rho c_L}\right)^{\frac{1}{\alpha_L}}} \frac{\beta^2\, x^{3+k} e^{-\beta x}}{1-e^{-\beta R}(\beta R+1)} dx \tag{31}$$

$$\mathbb{V}_{d2d,N} = \frac{1}{4\pi^2\tau_L}\left(\theta_u M_u^{\frac{2+k}{\alpha_N}} + (2\pi-\theta_u)m_u^{\frac{2+k}{\alpha_N}}\right)^2 \frac{\Gamma\left(m_N+\frac{2+k}{\alpha_N}\right)}{\Gamma(m_N)}\left(\frac{\rho m_N c_L}{M_u^2}\right)^{\frac{2+k}{\alpha_N}} \int_{x=0}^{\left(\frac{P_{d2d}M_u^2}{\rho c_L}\right)^{\frac{1}{\alpha_L}}} \frac{\beta^2 x^{1+\frac{\alpha_L(2+k)}{\alpha_N}} e^{-\beta x}}{1-e^{-\beta R}(\beta R+1)} dx \tag{32}$$

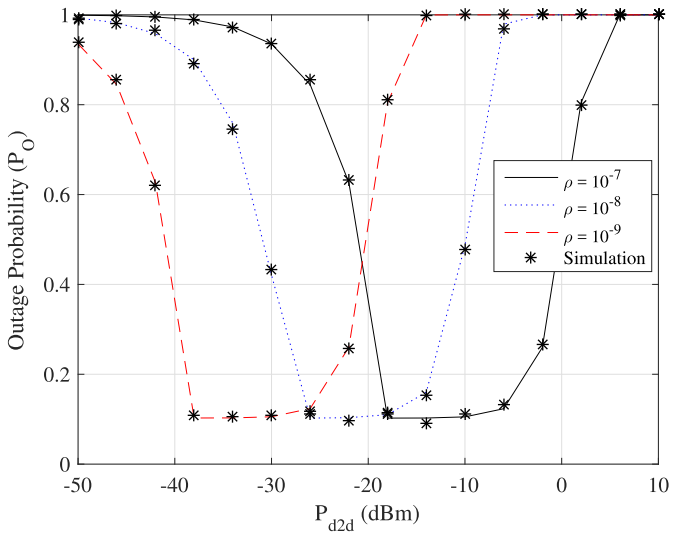

Fig. 4. The outage probability (P_O) vs. the peak D2D power level P_{d2d} for nearest association under different receiver thresholds ρ. $\gamma_{th} = 10^{-3}$, $R = 100$, and $M_u = 20$ dB, $m_L = 2$, $m_N = 1$, and $\lambda_{d,t} = 10^{-4}$.

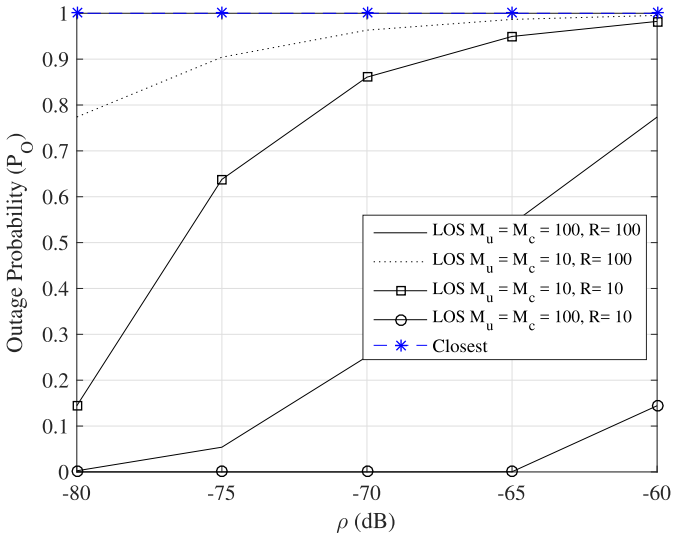

Fig. 5. The outage probability vs. the receiver sensitivity ρ for LOS association under different antenna gains and D2D cluster radii, and closest association. It should be noted that the curves for closest association overlap. $\beta = 0.1$, $\gamma_{th} = 10^{-3}$, and $P_{d2d} = 10^{-3}$.

We investigate the effect of the peak D2D transmit power P_{d2d} on the outage in Fig. 4. While P_{d2d} increases, the outage first drops, and then approaches 1. As such, there is an optimum P_{d2d} which gives the best performance. Furthermore, it is observed that a change in the receiver sensitivity ρ does not significantly change the performance characteristics except shifting the location of the minimum outage; a higher ρ provides the best performance at a higher P_{d2d} and vice-versa.

We will next consider the LOS association and compare it with the closest association. First, the outage probability is plotted against the receiver sensitivity ρ in Fig. 5. It is seen that the outage increases with ρ. When ρ increases, two effects may happen. If the threshold transmit power P_{d2d} is high enough, the increased transmit power from D2D transmitters

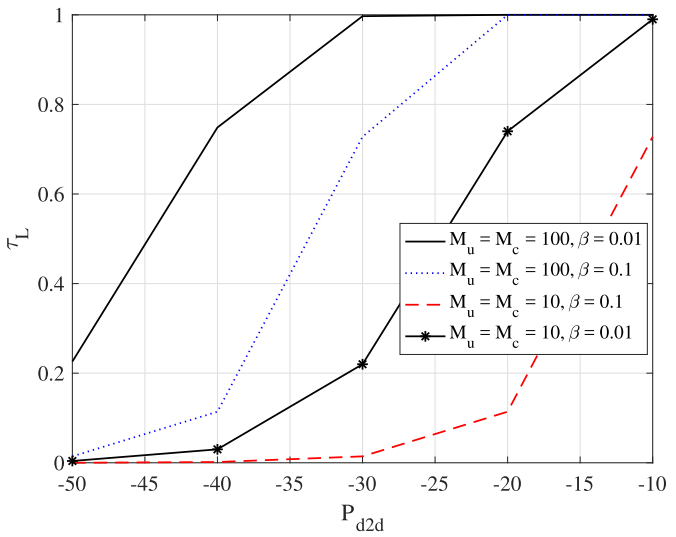

Fig. 6. The probability of D2D transmission (τ_L) for LOS association vs. the D2D cut-off threshold P_{d2d} under different antenna gains and blockage parameter (β) values.

will increase interference. On the other hand, for lower P_{d2d}, increasing ρ means that the required transmit power is more likely to exceed the threshold. Thus, the interference is lower. However, this cut-off affects the desired link as well, which increases the outage. It is also seen that when the main lobe gains of the antennas increase to 20 dB from 10 dB, the outage drops considerably. With higher antenna gains, the required transmit power is lower for the desired link, and there is a lower probability that it will get cut-off. This offsets any increased interference from other co-channel D2D users. As similar effect occurs when the D2D cluster radius is increased. For high R, the required transmit power on the desired link is high, and thus the link can get easily cut-off due to the peak power threshold. Therefore, it can be concluded that the effects of antenna gains and cluster radii on the desired link is far more important compared to their affect on the interfering signals. The curves for closest association all overlap under the parameters uses, and the outage probability is closes to 1. As we have used a high value for β ($\beta = 0.1$), all links have a higher tendency for blockage As such, the LOS association scheme performs significantly better with respect to the D2D outage compared with closest association in adverse environments with multiple obstacles.

As our final figure, we plot the probability of D2D transmission τ_L as a function of D2D peak cut-off threshold P_{d2d} in Fig. 6. We can think of τ_L as a rough measure of D2D link capacity. While τ_L increases universally with P_{d2d} for all antenna gains and β, they have different characteristics. Intuitively, a higher cut-off threshold allows more D2D transmissions to continue unhindered, and $\tau_L \rightarrow 1$ if P_{d2d} is increased sufficiently. Moreover, a higher antenna gain results in increased D2D link capacity because D2D transmitter is less likely to be cut-off due to lower required transmit powers. In addition, a higher blockage parameter β results in less D2D link capacity (e.g., lower τ_L).

VI. Conclusion

The outage performance of a random D2D network underlaying a millimeter wave cellular network was characterized. Homogeneous Poisson processes were considered for the locations of the cellular base stations and users while a Matérn cluster process was considered for the locations of the D2D network nodes. Sectored antenna patterns and random blockages were considered alongside different path loss exponents and Nakagami fading indexes depending on the LOS or NLOS nature of a link. Two association schemes were considered. First, the cellular users were assumed to connect with their closest base station while D2D transmitters connect with a random receiver within its cluster. Second, the cellular users were assumed to connect with their closest LOS base station wile D2D transmitters connected with a random LOS receivers within their respective clusters. Moreover, path loss and antenna gain inversion based power control which vary upon the LOS or NLOS nature is employed by both networks while D2D transmitters are also peak power constrained.

The MGFs of interference on a D2D receiver device from the cellular base stations and other D2D transmitters are derived in closed-form, and are used to obtain the outage probability of a D2D receiver. While the derived expressions generally complicated, they can be readily evaluated to provide valuable system specific insights. It is observed that the outage has a complex relationship with the D2D cluster radius and antenna gains. Furthermore, a minima of the outage is occurs for a specific D2D peak power threshold, while a higher LOS fading severity (lower m_L) also reduces the outage. It is also concluded that the cut-off probability of the desired link is the main contributor to the outage compared with the co-channel interference and noise. Changes to parameters such as the receiver sensitivity, peak power threshold, and the D2D cluster radius can adversely affect the outage of a typical D2D receiver even though the same changes actually limit interference. Depending on the receiver sensitivity, the peak power threshold P_{d2d} can be judiciously selected to ensure a minimum outage and maximum performance. It should also be noted that in adverse environments with a high chance of blockage, the LOS association scheme may yield better results. Extensions of the work include alternate transmitter-receiver association schemes, power control schemes, and antenna misalignment effects. Moreover, developing strategies to characterize the optimum P_{d2d} and R which minimize outage are exciting future challenges.

Appendix
Proof of expressions

A. Proof of $P_{O,L}$

We can write

$$P_{O,L} = \Pr\left[\frac{P_L|h_L|^2 M_u^2 c_L^{-1} r_{d2d}^{-\alpha_L}}{I_c + I_{d2d} + N} < \gamma_{th}\right]. \tag{33}$$

The transmit power P_L is given by

$$P_L = \begin{cases} \dfrac{\rho c_L r_{d2d}^{\alpha_L}}{M_u^2}, & \dfrac{\rho c_L r_{d2d}^{\alpha_L}}{M_u^2} < P_{d2d} \\ 0, & \text{otherwise.} \end{cases} \tag{34}$$

Let τ_L be the probability that $P_L = \frac{\rho c_L r_{d2d}^{\alpha_L}}{M_u^2}$. Thus, we can express $\tau_L = \Pr\left[r_{d2d} < \left(\frac{P_{d2d}M_u^2}{\rho c_L}\right)^{\frac{1}{\alpha_L}}\right]$ as

$$\tau_L = \begin{cases} \dfrac{1}{R^2}\left(\dfrac{P_{d2d}M_u^2}{\rho c_L}\right)^{\frac{2}{\alpha_L}}, & \text{if } \left(\dfrac{P_{d2d}M_u^2}{\rho c_L}\right)^{\frac{1}{\alpha_L}} < R \\ 1, & \text{if } \left(\dfrac{P_{d2d}M_u^2}{\rho c_L}\right)^{\frac{1}{\alpha_L}} > R. \end{cases} \tag{35}$$

Now, getting back to the objective of deriving $P_{O,L}$, we can express (33) for integer m_l as

$$\begin{aligned}
&P_{O,L} \\
&= 1 - \tau_L + \tau_L \Pr\left[|h_L|^2 < \frac{\gamma_{th}(I_c + I_{d2d} + N)}{\rho}\right] \\
&= 1 - \tau_L \mathbb{E}\left[\frac{\Gamma\left(m_L, m_L\frac{\gamma_{th}(I_c+I_{d2d}+N)}{\rho}\right)}{\Gamma(m_L)}\right] \\
&= 1 - \tau_L \mathbb{E}_I\left[\frac{1}{\Gamma(m_L)}\int_{\frac{m_L\gamma_{th}(I_c+I_{d2d}+N)}{\rho}}^{\infty} y^{m_L-1}e^{-y}dy\right] \\
&= 1 - \tau_L \mathbb{E}_I\Bigg[e^{-\frac{m_L\gamma_{th}(I_c+I_{d2d}+N)}{\rho}} \\
&\quad \times \sum_{\nu=0}^{m_L-1}\frac{1}{\nu!}\left(\frac{m_L\gamma_{th}(I_c+I_{d2d}+N)}{\rho}\right)^{\nu}\Bigg] \\
&= 1 - \tau_L e^{-\frac{m_L\gamma_{th}N}{\rho}}\sum_{\nu=0}^{m_L-1}\frac{1}{\nu!}\left(\frac{m_L\gamma_{th}}{\rho}\right)^{\nu}\sum_{\mu=0}^{\nu}\binom{\nu}{\mu}N^{\nu-\mu} \\
&\quad \times \sum_{\kappa=0}^{\mu}\binom{\mu}{\kappa}\mathbb{E}_{I_c}\left[I_c^{\kappa}e^{-\frac{m_L\gamma_{th}I_c}{\rho}}\right]\mathbb{E}_{I_{d2d}}\left[I_{d2d}^{\mu-\kappa}e^{-\frac{m_L\gamma_{th}I_{d2d}}{\rho}}\right] \\
&= 1 - \tau_L e^{-\frac{m_L\gamma_{th}N}{\rho}}\sum_{\nu=0}^{m_L-1}\frac{1}{\nu!}\left(\frac{m_L\gamma_{th}}{\rho}\right)^{\nu} \\
&\quad \times \sum_{\mu=0}^{\nu}\binom{\nu}{\mu}N^{\nu-\mu}\sum_{\kappa=0}^{\mu}\binom{\mu}{\kappa}(-1)^{\kappa}M_{I_c}^{(\kappa)}\left(s|_{s=\frac{m_L\gamma_{th}}{\rho}}\right) \\
&\quad \times (-1)^{\mu-\kappa}M_{I_{d2d}}^{(\mu-\kappa)}\left(s|_{s=\frac{m_L\gamma_{th}}{\rho}}\right).
\end{aligned} \tag{36}$$

B. Proof of $M_{I_{c,L}}$

In order to derive $M_{I_{c,L}}$ we first transform the process of interfering LOS base stations to an equivalent inhomogeneous Poisson point process which incorporates the path loss exponent, antenna gains, transmit power, and fading. Let r be the distance from the i-th cellular base station $\phi_{c,b}^i$ to the considered D2D receiver. While the field of cellular base stations $\Phi_{c,b}$ exists in $\mathbb{R}^2$ as a homogeneous Poisson point process, it can be mapped to an equivalent 1-D inhomogeneous Poisson point process [49] with density $\tilde{\lambda}_{c,b}$ where

$$\tilde{\lambda}_{c,b} = 2\pi\lambda_{c,b}r, \quad 0 \le r < \infty. \tag{37}$$

The cellular base station $\phi_{c,b}^i$ is LOS from the D2D receiver with a probability of $e^{-\beta r}$. While this probability depends on r, it is independent from the positions of other cellular base stations. Moreover, it should be noted that the mapping process does not affect the LOS/NLOS nature of a transmitter receiver

link as the distance properties remain unchanged. Keeping these facts in mind, the Colouring Theorem [49] can be used to perform independent thinning of $\Phi_{c,b}$ to obtain the process of LOS cellular base stations as an inhomogeneous Poisson point process with density $\tilde{\lambda}_{c,bL} = e^{-\beta r}\tilde{\lambda}_{c,b} = 2\pi\lambda_{c,b}e^{-\beta r}r$.

Using the Mapping Theorem further [49], this thinned 1-D Poisson process can be mapped to an equivalent 1-D Poisson process in terms of interference statistics where the path loss exponent is 1 [42]. The density of the resultant process $\hat{\lambda}_{c,bL}$ is given by

$$\hat{\lambda}_{c,bL} = \frac{2\pi\lambda_{c,b}e^{-\beta r^{\frac{1}{\alpha_L}}} r^{\frac{2}{\alpha_L}-1}}{\alpha_L}, \quad 0 \leq r < \infty. \tag{38}$$

Next, we go one step further and incorporate the transmit power of $\phi^i_{c,b}$, the antenna gains of $\phi^i_{c,b}$ and the D2D receiver, and the fading between $\phi^i_{c,b}$ and the D2D receiver to the process of LOS cellular base stations [42]. Thus, the resultant process has a density $\bar{\lambda}_{c,bL}$ which can be expressed as

$$\begin{aligned}
&\bar{\lambda}_{c,bL} \\
&= \mathbb{E}_{P_{cL}G_{cb}G_u|h_{cL}|^2}\left[P_{cL}|h_{cL}|^2\hat{\lambda}_{c,bL}(P_{cL}G_{cb}G_u|h_{cL}|^2\ r)\right] \\
&= \frac{2\pi\lambda_{c,b}r^{\frac{2}{\alpha_L}-1}}{\alpha_L}\sum_{k=0}^{\infty}\frac{(-\beta r^{\frac{1}{\alpha_L}})^k}{k!} \\
&\quad \times \mathbb{E}\left[P_{cL}^{\frac{2+k}{\alpha_L}}\right]\mathbb{E}\left[G_{cb}^{\frac{2+k}{\alpha_L}}\right]\mathbb{E}\left[G_u^{\frac{2+k}{\alpha_L}}\right]\mathbb{E}\left[(|h_{cL}|^2)^{\frac{2+k}{\alpha_L}}\right],
\end{aligned} \tag{39}$$

where P_{cL} is the transmit power of the base station $\phi^i_{c,b}$, G_{cb} is the gain of $\phi^i_{c,b}$, G_u is the gain of the D2D receiver, and $|h_{cL}|^2$ is the small scale fading channel gain between $\phi^i_{c,b}$ and the D2D receiver.

From (3), $\mathbb{E}_{G_{cb}}\left[G_{cb}^{\frac{2+k}{\alpha_L}}\right]$ and $\mathbb{E}_{G_u}\left[G_u^{\frac{2+k}{\alpha_L}}\right]$ are obtained as

$$\begin{aligned}
\mathbb{E}_{G_{cb}}\left[G_{cb}^{\frac{2+k}{\alpha_L}}\right] &= \frac{1}{2\pi}\left(\theta_{cb}M_{cb}^{\frac{2+k}{\alpha_L}} + (2\pi-\theta_{cb})m_{cb}^{\frac{2+k}{\alpha_L}}\right) \\
\mathbb{E}_{G_u}\left[G_u^{\frac{2+k}{\alpha_L}}\right] &= \frac{1}{2\pi}\left(\theta_{u}M_{u}^{\frac{2+k}{\alpha_L}} + (2\pi-\theta_{u})m_{u}^{\frac{2+k}{\alpha_L}}\right),
\end{aligned} \tag{40}$$

while $\mathbb{E}_{|h_{cL}|^2}\left[(|h_{cL}|^2)^{\frac{2+k}{\alpha_L}}\right]$ is obtained from (2) as

$$\mathbb{E}_{|h_{cL}|^2}\left[(|h_{cL}|^2)^{\frac{2+k}{\alpha_L}}\right] = \frac{m_L^{\frac{2+k}{\alpha_L}}\Gamma\left(m_L+\frac{2+k}{\alpha_L}\right)}{\Gamma(m_L)}. \tag{41}$$

Moreover, in order to evaluate (39), the distribution of P_{cL} is required, which in turn depends on whether the associated cellular user to $\phi^i_{c,b}$ is within LOS or not. The associated receiver $\phi^i_{c,u}$ is LOS to $\phi^i_{c,b}$ with probability $e^{-\beta r_c}$, and NLOS with probability $1-e^{-\beta r_c}$, where r_c is the distance between $\phi^i_{c,u}$ and $\phi^i_{c,b}$. These probabilities are independent from whether $\phi^i_{c,b}$ and the D2D receiver are LOS or not. Thus, P_{cL} can be expressed as follows:

$$P_{cL} = \begin{cases} \dfrac{\rho c_L r_c^{\alpha_L}}{M_U M_{cb}}, & \phi^i_{c,u} \text{ and } \phi^i_{c,b} \text{ are LOS} \\ \dfrac{\rho c_N r_c^{\alpha_N}}{M_U M_{cb}}, & \phi^i_{c,u} \text{ and } \phi^i_{c,b} \text{ are NLOS.} \end{cases} \tag{42}$$

After substituting $\mathbb{E}_{|h_{cL}|^2}\left[(|h_{cL}|^2)^{\frac{2+k}{\alpha_L}}\right]$, $\mathbb{E}_{P_{cL}}\left[P_{cL}^{\frac{2+k}{\alpha_L}}\right]$, $\mathbb{E}_{G_{cb}}\left[G_{cb}^{\frac{2+k}{\alpha_L}}\right]$, and $\mathbb{E}_{G_u}\left[G_u^{\frac{2+k}{\alpha_L}}\right]$ to (39), we obtain the final expression for $\bar{\lambda}_{c,bL}$ as

$$\bar{\lambda}_{c,bL} = \sum_{k=0}^{\infty}\frac{2\pi\lambda_{c,b}(-\beta)^k r^{\frac{2+k}{\alpha_L}-1}}{\alpha_L k!}\mathbb{U}_{c,L}, \quad 0 < r < \infty, \tag{43}$$

where $\mathbb{U}_{c,L}$ is given in (12), as shown at the bottom of the fifth page.

We now return to our origin objective of deriving $M_{I_{c,L}} = \mathbb{E}[e^{-sI_{c,L}}]$. Due to the mapping, the interference power from a single cellular base station $\phi^i_{c,b}$ within the resultant process reduces to $(c_L r)^{-1}$. Note that the path loss exponent has reduced to 1 while the gains, fading, and transmit powers are absent. Thus, using the Campbell's Theorem [49], $M_{I_{c,L}}$ is expressed as

$$\begin{aligned}
M_{I_{c,L}} &= e^{\left(\int_0^\infty\left(e^{-s(c_L r)^{-1}}-1\right)\bar{\lambda}_{c,bL}dr\right)} \\
&= e^{\sum_{k=0}^{\infty}\frac{2\pi\lambda_{c,b}(-\beta)^k}{\alpha_L k!}\left(\frac{s}{c_L}\right)^{\frac{2+k}{\alpha_L}}\Gamma\left(-\frac{2+k}{\alpha_L}\right)\mathbb{U}_{c,L}}.
\end{aligned} \tag{44}$$

C. Proof of $f_{r_c}(x)$

Each cellular user associates with its nearest LOS base station. For a typical cellular user, it sees the PPP of cellular base stations $\Phi_{c,b}$ as a 2-D homogeneous PPP with uniform intensity $\lambda_{c,b}$. Using the mapping theorem of PPPs [49] this can be equivalently written as a 1-D PPP with intensity [49]

$$\lambda^{1D}_{c,b} = 2\pi\lambda_{c,b}r, \quad 0 < r < \infty, \tag{45}$$

where r is the distance from any cellular user. However, we only require the base stations which are LOS. The fact whether a base station is LOS or NLOS depends only on the distance r, and not on the locations of other base stations. As such, independent thinning [49] can be employed on $\Phi_{c,b}$ by marking each base station on whther it is blocked or not to obtain the process of LOS base stations. If $\Phi^{LOS}_{c,b}$ is the process of the LOS base stations, its intensity is given by

$$\lambda^{LOS}_{c,b} = 2\pi\lambda_{c,b}re^{-\beta r}, \quad 0 < r < \infty. \tag{46}$$

Using (46) and (1), we can obtain the CDF of the distance from a typical cellular user to its closest LOS base station by calculating the void probability. This procedure makes use of the fact that if the closest base station is within a distance of x, there will not be a case of 0 base stations within that distance. Thus, the CDF is written as

$$F_{r_c}(x) = 1 - e^{-\frac{2\pi\lambda_{c,b}}{\beta^2}(1-e^{-\beta x}(\beta x+1))}, \quad 0 < r < \infty. \tag{47}$$

Differentiating this gives the PDF which is

$$f_{r_c}(x) = 2\pi\lambda_{c,b}xe^{-\frac{2\pi\lambda_{c,b}}{\beta^2}(1-e^{-\beta x}(\beta x+1))-\beta x}, \quad 0 < r < \infty.$$

D. Proof of $f_{r_{d2d}}(x)$

Each D2D transmitter associates with a random LOS receiver within its cluster, which has a radius of R. The receivers (whether LOS or NLOS) form a 2-D homogeneous PPP surrounding a D2D transmitter, and this can be equivalently transformed to a 1-D PPP with intensity

$$\lambda_{d2d}^{1D} = 2\pi\lambda_{d,r} r, \quad 0 < r < R. \tag{48}$$

Similar to the derivation of $f_{r_c}(x)$, the LOS receivers form a thinned PPP with intensity

$$\lambda_{d2d}^{LOS} = 2\pi\lambda_{d,r} r e^{-\beta r}, \quad 0 < r < R. \tag{49}$$

With (49), the CDF of the distance from a D2D transmitter to the associated receiver r_{d2d} can be written as

$$\begin{aligned} F_{r_{d2d}}(x) &= \frac{\int_{r=0}^{x} 2\pi\lambda_{d,r} r e^{-\beta r} dr}{\int_{r=0}^{x} 2\pi\lambda_{d,r} r e^{-\beta r} dr} \\ &= \frac{1 - e^{-\beta x}(\beta x + 1)}{1 - e^{-\beta R}(\beta R + 1)}, \quad 0 < r < R. \end{aligned} \tag{50}$$

Differentiating this result gives the PDF as

$$f_{r_{d2d}}(x) = \frac{\beta^2 x e^{-\beta x}}{1 - e^{-\beta R}(\beta R + 1)}, \quad 0 < r < R. \tag{51}$$

REFERENCES

[1] S. Kusaladharma and C. Tellambura, "Interference and outage in random D2D networks under millimeter wave channels," in *Proc. IEEE ICC*, May 2017, pp. 1–7.

[2] O. Y. Kolawole, S. Vuppala, and T. Ratnarajah, "Multiuser millimeter wave cloud radio access networks with hybrid precoding," *IEEE Syst. J.*, to be published.

[3] D. Liu *et al.*, "User association in 5G networks: A survey and an outlook," *IEEE Commun. Surveys Tuts.*, vol. 18, no. 2, pp. 1018–1044, 2nd Quart., 2016.

[4] T. S. Rappaport *et al.*, "Millimeter wave mobile communications for 5G cellular: It will work!" *IEEE Access*, vol. 1, pp. 335–349, May 2013.

[5] J. G. Andrews, T. Bai, M. N. Kulkarni, A. Alkhateeb, A. K. Gupta, and R. W. Heath, Jr., "Modeling and analyzing millimeter wave cellular systems," *IEEE Trans. Commun.*, vol. 65, no. 1, pp. 403–430, Jan. 2017.

[6] W. Lu and M. Di Renzo, "Stochastic geometry modeling of mmWave cellular networks: Analysis and experimental validation," in *Proc. IEEE IWMN*, Oct. 2015, pp. 1–4.

[7] S. Mumtaz, J. Rodriguez, and L. Dai, *mmWave Massive MIMO: A Paradigm for 5G*, 1st ed. New York, NY, USA: Academic, 2016.

[8] T. Bai and R. W. Heath, Jr., "Coverage and rate analysis for millimeter-wave cellular networks," *IEEE Trans. Wireless Commun.*, vol. 14, no. 2, pp. 1100–1114, Feb. 2015.

[9] T. A. Khan, A. Alkhateeb, and R. W. Heath, Jr., "Millimeter wave energy harvesting," *IEEE Trans. Wireless Commun.*, vol. 15, no. 9, pp. 6048–6062, Sep. 2016.

[10] S. He, J. Wang, Y. Huang, B. Ottersten, and W. Hong, "Codebook-based hybrid precoding for millimeter wave multiuser systems," *IEEE Trans. Signal Process.*, vol. 65, no. 20, pp. 5289–5304, Oct. 2017.

[11] C.-X. Wang *et al.*, "Cellular architecture and key technologies for 5G wireless communication networks," *IEEE Commun. Mag.*, vol. 52, no. 2, pp. 122–130, Feb. 2014.

[12] J. Qiao, X. Shen, J. Mark, Q. Shen, Y. He, and L. Lei, "Enabling device-to-device communications in millimeter-wave 5G cellular networks," *IEEE Commun. Mag.*, vol. 53, no. 1, pp. 209–215, Jan. 2015.

[13] N. Deng and M. Haenggi, "A fine-grained analysis of millimeter-wave device-to-device networks," *IEEE Trans. Commun.*, vol. 65, no. 11, pp. 4940–4954, Nov. 2017.

[14] A. Gupta and E. R. K. Jha, "A survey of 5G network: Architecture and emerging technologies," *IEEE Access*, vol. 3, pp. 1206–1232, Jul. 2015.

[15] M. Afshang, H. S. Dhillon, and P. H. J. Chong, "Modeling and performance analysis of clustered device-to-device networks," *IEEE Trans. Wireless Commun.*, vol. 15, no. 7, pp. 4957–4972, Jul. 2016.

[16] H. Ding, X. Wang, D. B. da Costa, and J. Ge, "Interference modeling in clustered device-to-device networks with uniform transmitter selection," *IEEE Trans. Wireless Commun.*, vol. 16, no. 12, pp. 7906–7918, Dec. 2017.

[17] D. Maamari, N. Devroye, and D. Tuninetti, "Coverage in mmWave cellular networks with base station co-operation," *IEEE Trans. Wireless Commun.*, vol. 15, no. 4, pp. 2981–2994, Apr. 2016.

[18] W. Lu and M. Di Renzo, "Accurate stochastic geometry modeling and analysis of mmWave cellular networks," in *Proc. IEEE ICUWB*, Oct. 2015, pp. 1–5.

[19] M. N. Kulkarni, J. G. Andrews, and A. Ghosh, "Performance of dynamic and static TDD in self-backhauled millimeter wave cellular networks," *IEEE Trans. Wireless Commun.*, vol. 16, no. 10, pp. 6460–6478, Oct. 2017.

[20] X. Zhou, S. Durrani, and J. Guo, "Characterization of aggregate received power from power beacons in millimeter wave ad hoc networks," in *Proc. IEEE ICC*, May 2017, pp. 1–7.

[21] M. Di Renzo, W. Lu, and P. Guan, "The intensity matching approach: A tractable stochastic geometry approximation to system-level analysis of cellular networks," *IEEE Trans. Wireless Commun.*, vol. 15, no. 9, pp. 5963–5983, Sep. 2016.

[22] X. Zhou, J. Guo, S. Durrani, and M. Di Renzo, "Power beacon-assisted millimeter wave ad hoc networks," *IEEE Trans. Commun.*, vol. 66, no. 2, pp. 830–844, Feb. 2018.

[23] K. Venugopal, M. C. Valenti, and R. W. Heath, Jr., "Device-to-device millimeter wave communications: Interference, coverage, rate, and finite topologies," *IEEE Trans. Wireless Commun.*, vol. 15, no. 9, pp. 6175–6188, Sep. 2016.

[24] Y. Niu *et al.*, "Exploiting device-to-device communications to enhance spatial reuse for popular content downloading in directional mmWave small cells," *IEEE Trans. Veh. Technol.*, vol. 65, no. 7, pp. 5538–5550, Jul. 2016.

[25] M. Mirahsan, R. Schoenen, S. S. Szyszkowicz, and H. Yanikomeroglu, "Measuring the spatial heterogeneity of outdoor users in wireless cellular networks based on open urban maps," in *Proc. IEEE ICC*, Jun. 2015, pp. 2834–2838.

[26] S. Wu, R. Atat, N. Mastronarde, and L. Liu, "Coverage analysis of D2D relay-assisted millimeter-wave cellular networks," in *Proc. IEEE WCNC*, Mar. 2017, pp. 1–6.

[27] Z. Guizani and N. Hamdi, "mmwave E-band D2D communications for 5G-underlay networks: Effect of power allocation on D2D and cellular users throughputs," in *Proc. IEEE ISCC*, Jun. 2016, pp. 114–118.

[28] M. Di Renzo and W. Lu, "System-level analysis and optimization of cellular networks with simultaneous wireless information and power transfer: Stochastic geometry modeling," *IEEE Trans. Veh. Technol.*, vol. 66, no. 3, pp. 2251–2275, Mar. 2017.

[29] I. Gradshteyn and I. Ryzhik, *Table of Integrals, Series, and Products*, 7th ed. New York, NY, USA: Academic, 2007.

[30] Z. Chen *et al.*, "Aggregate interference modeling in cognitive radio networks with power and contention control," *IEEE Trans. Commun.*, vol. 60, no. 2, pp. 456–468, Feb. 2012.

[31] E. Salbaroli and A. Zanella, "Interference analysis in a Poisson field of nodes of finite area," *IEEE Trans. Veh. Technol.*, vol. 58, no. 4, pp. 1776–1783, May 2009.

[32] A. Baddeley, I. Barany, R. Schneider, and W. Weil, "Spatial point processes and their applications," in *Stochastic Geometry*. Berlin, Germany: Springer, 2007.

[33] Y. Liu, C. Yin, J. Gao, and X. Sun, "Transmission capacity for overlaid wireless networks: A homogeneous primary network versus an inhomogeneous secondary network," in *Proc. IEEE ICCCAS*, vol. 1, Nov. 2013, pp. 154–158.

[34] T. Bai, R. Vaze, and R. W. Heath, Jr., "Analysis of blockage effects on urban cellular networks," *IEEE Trans. Wireless Commun.*, vol. 13, no. 9, pp. 5070–5083, Sep. 2014.

[35] M. Di Renzo, "Stochastic geometry modeling and analysis of multi-tier millimeter wave cellular networks," *IEEE Trans. Wireless Commun.*, vol. 14, no. 9, pp. 5038–5057, Sep. 2015.

[36] G. R. MacCartney, J. Zhang, S. Nie, and T. S. Rappaport, "Path loss models for 5G millimeter wave propagation channels in urban microcells," in *Proc. IEEE GLOBECOM*, Dec. 2013, pp. 3948–3953.

[37] C. Tellambura, A. Annamalai, and V. K. Bhargava, "Closed form and infinite series solutions for the MGF of a dual-diversity selection combiner output in bivariate Nakagami fading," *IEEE Trans. Commun.*, vol. 51, no. 4, pp. 539–542, Apr. 2003.

[38] A. Molisch, *Wireless Communications*. Hoboken, NJ, USA: Wiley, 2011.

[39] X. Wu *et al.*, "60-GHz millimeter-wave channel measurements and modeling for indoor office environments," *IEEE Trans. Antennas Propag.*, vol. 65, no. 4, pp. 1912–1924, Apr. 2017.

[40] M. R. Akdeniz *et al.*, "Millimeter wave channel modeling and cellular capacity evaluation," *IEEE J. Sel. Areas Commun.*, vol. 32, no. 6, pp. 1164–1179, Jun. 2014.
[41] N. A. Muhammad, P. Wang, Y. Li, and B. Vucetic, "Analytical model for outdoor millimeter wave channels using geometry-based stochastic approach," *IEEE Trans. Veh. Technol.*, vol. 66, no. 2, pp. 912–926, Feb. 2017.
[42] S. Kusaladharma, P. Herath, and C. Tellambura, "Underlay interference analysis of power control and receiver association schemes," *IEEE Trans. Veh. Technol.*, vol. 65, no. 11, pp. 8978–8991, Nov. 2016.
[43] S. Kusaladharma and C. Tellambura, "Massive MIMO based underlay networks with power control," in *Proc. IEEE ICC*, May 2016, pp. 1–6.
[44] S. Kusaladharma and C. Tellambura, "Aggregate interference analysis for underlay cognitive radio networks," *IEEE Wireless Commun. Lett.*, vol. 1, no. 6, pp. 641–644, Dec. 2012.
[45] C. Tellambura, A. J. Mueller, and V. K. Bhargawa, "Analysis of M-ary phase-shift keying with diversity reception for land-mobile satellite channels," *IEEE Trans. Veh. Technol.*, vol. 46, no. 4, pp. 910–922, Nov. 1997.
[46] C. Tellambura, "Evaluation of the exact union bound for trellis-coded modulations over fading channels," *IEEE Trans. Commun.*, vol. 44, no. 12, pp. 1693–1699, Dec. 1996.
[47] S. Kusaladharma, P. Herath, and C. Tellambura, "Secondary user interference characterization for underlay networks," in *Proc. IEEE VTC*, Sep. 2015, pp. 1–5.
[48] S. Kusaladharma and C. Tellambura, "On approximating the cognitive radio aggregate interference," *IEEE Wireless Commun. Lett.*, vol. 2, no. 1, pp. 58–61, Feb. 2013.
[49] J. F. C. Kingman, *Poisson Processes*. London, U.K.: Oxford Univ. Press, 1993.

Sachitha Kusaladharma received the B.Sc. degree (Hons.) in electrical and telecommunication engineering from the University of Moratuwa, Moratuwa, Sri Lanka, in 2010, and the M.Sc. and Ph.D. degrees in electrical and computer engineering from the University of Alberta, Edmonton, AB, Canada, in 2013 and 2017, respectively. Since 2017, he has been a Post-Doctoral Fellow at Concordia University, Canada. His research interests include cognitive radio networks, communication theory, multiple-input multiple-output systems, and wireless sensor networks. He received the Alberta Innovates Technology Futures Graduate Student Scholarship in 2013.

Zhang Zhang received the B.Eng. and Ph.D. degrees from the Beijing University of Posts and Telecommunications, Beijing, China, in 2007 and 2012, respectively. From 2009 to 2012, he was a Research Assistant with the Wireless and Mobile Communications Technology Research and Development Center, Tsinghua University, Beijing. He is currently with the Department of Radio Access Network Research, Huawei Technologies Co., Ltd, Shanghai, China. His current research interests include information theory and radio access technologies.

Chintha Tellambura (F'11) received the B.Sc. degree (Hons.) from the University of Moratuwa, Sri Lanka, in 1986, the M.Sc. degree in electronics from King's College London, U.K., in 1988, and the Ph.D. degree in electrical engineering from the University of Victoria, Canada, in 1993.

He was with Monash University, Australia, from 1997 to 2002. He is currently a Professor with the Department of Electrical and Computer Engineering, University of Alberta. His current research interests include the design, modeling, and analysis of cognitive radio, heterogeneous cellular networks, and 5G wireless networks.

He has authored or co-authored over 500 journal and conference papers with total citations over 14 000 and an h-index of 62 on Google Scholar. In 2011, he was elected as an IEEE Fellow for his contributions to physical layer wireless communication theory, and in 2017, elected as a fellow of the Canadian Academy of Engineering. He received the best paper awards from the Communication Theory Symposium in 2012, the IEEE International Conference on Communications (ICC) in Canada, and the 2017 ICC in France. He was a recipient of the prestigious McCalla Professorship and the Killam Annual Professorship from the University of Alberta. He served as an Editor for the IEEE TRANSACTIONS ON COMMUNICATIONS (1999–2011). From 2001 to 2007, he was an Editor for the IEEE TRANSACTIONS ON WIRELESS COMMUNICATIONS and continued as an Area Editor for Wireless Communications Systems and Theory from 2007 to 2012.